scientific reports

OPEN

Unveiling islet heterogeneity using an automated microfluidic imaging system

James Thornham[1], Richard Bertram[1,2,3] & Michael G. Roper[1,4✉]

Islets of Langerhans are a therapeutic target for diabetes and prediabetes. Measurements of therapeutic inhibitory or excitatory concentrations are often performed using large groups of islets, however, the population heterogeneity cannot be observed when examining the ensemble response. Normal islet function and islet response to therapeutic treatment can be affected by islet heterogeneity, influencing the progression of diabetes mellitus. To identify heterogeneity in an islet population, we developed a simple microfluidic device capable of delivering a stimulant to four independent chambers, allowing measurements of individual responses from a population of 20–25 islets. The device enabled accurate delivery of the same stimulant concentration to all four chambers, with an error <1% between chambers. To demonstrate the capability of this system, ensemble and individual EC/IC_{50} measurements of glucose and diazoxide were performed on murine islets. Results showed little heterogeneity of glucose EC_{50} values with all 21 islets within $\pm$ 0.6 mM of the ensemble value of 7.4 mM. In contrast, application of diazoxide to 24 islets in the presence of 20 mM glucose resulted in 37% of islets having an IC_{50} greater than 10% from the ensemble value of 10.2 μM. The simple system developed here is amenable to further studies on islet heterogeneity, and is applicable to investigate heterogeneity in other cell types.

Diabetes mellitus is characterized by the loss of proper blood glucose regulation and currently affects 38.4 million people in the United States. Of those with the disease, 95% have type 2 diabetes mellitus (T2DM)[1]. In a healthy person, glucose is regulated by the secretion of insulin from islets of Langerhans. Islets are pancreatic micro-organs comprised of multiple cell types, including β cells, the only insulin secreting cell type in the body[2]. As such, islets have long been a target for T2DM therapeutics[3]. Understanding the response of islets to potential therapeutics is critical for the continued development of these compounds.

Commonly, functional response is determined by placing groups of islets into either tubes and measuring the concentration of insulin in the supernatant before and after incubation with the compound of interest[4,5], or for dynamic measurements, perfused with effluent fractions collected and analyzed offline[4,6,7]. However, these approaches do not allow for observation of the individual islet responses to identify the functional heterogeneity of the population. Functional heterogeneity at the single islet or single cell level is well known and give rise to heterogeneous pulsatile insulin secretion profiles under stimulatory extracellular glucose conditions[8–12]. These pulsatile dynamics have been shown to be critical for efficient glucose uptake[13], further driving the need for methods that can reveal individual islet dynamics[14].

To facilitate observation of these dynamics, microfluidic devices have been used to study the response of islets to stimulants[15], inhibitors[16], and other extracellular[17] factors. Microfluidic systems are ideal for varying extracellular environments because they enable manipulation of small volumes of buffers in a rapid manner. Automated microfluidic approaches to investigate islet responses have been developed for single islets[18–22], arrays of islets[23–26], as well as integrated responses from groups[27–29] of islets. Although powerful, each of these devices has limitations. For example, single islet devices suffer from low throughput, arrayed devices rely on complicated microfabrication methods, and devices developed for small groups of islets do not allow for examination of individual responses. Therefore, there is a need for simple microfluidic systems which are capable of continuous single islet measurements under varying extracellular conditions.

In this report, we describe an evolution of our previous live cell imaging microfluidic systems[30–32]. A one-layer microfluidic device has been developed for maintaining a controlled extracellular environment during imaging of 20-25 individual islets. A gravity-driven perfusion system is used to tune concentrations of stimulants

[1]Program in Molecular Biophysics, Institute of Molecular Biophysics, Florida State University, Tallahassee, FL 32304, USA. [2]Department of Mathematics, Florida State University, Tallahassee, FL 32306, USA. [3]Program of Neuroscience, Florida State University, Tallahassee, FL 32306, USA. [4]Department of Chemistry and Biochemistry, Florida State University, Tallahassee, FL 32306, USA. ✉email: mroper@fsu.edu

delivered to 4 parallel islet imaging chambers. This microfluidic setup enables analysis of dynamic activity in single pancreatic islets of Langerhans under a controlled extracellular environment where the concentration of stimulants can be varied during the course of the experiment, providing insight into the heterogeneity of responses of a population as well as ensemble characteristics. Using this device, we have observed the response of murine islets to various glucose levels and investigated the heterogeneity of inhibitory diazoxide (Dz) on islet responses.

Results

The microfluidic device (Fig. 1) was designed to enable accurate and precise mixing of two input buffers generated on the microfluidic device to be delivered to four islet chambers being imaged. As shown on the right of Fig. 1, this was achieved using a mixing junction that combined two inlet solutions in a ratio determined by the flow rates from the inputs[30–34]. Flow through the device was driven by a gravity perfusion system where the inlet solution reservoirs were suspended above the microfluidic device, generating a hydrostatic pressure at the inlets which drove flow through the channels. A particular concentration of reagent was delivered to the islets by controlling the ratio of the two inlet flows. The resulting combination of buffers generated at the mixing junction flowed through a serpentine mixing channel, where they mixed to completion. By adjusting the height of the reservoirs above the device, the hydrostatic pressure and hence flow rates through the corresponding inlets were changed. For example, given an increased flow rate through inlet 1 on the left, the flow from inlet 2 will be reduced and sent primarily through the serpentine waste channel at the far right of the mixing junction to the common outlet, resulting in a new concentration delivered to the islets. By sufficiently increasing the flow rate from inlet 1, all of the flow from inlet 2 will be forced into the waste channel and only solution from inlet 1 will be delivered to the islets. To maintain a constant total pressure and flow rate in the device, when one reservoir was raised, the other was lowered by the same amount. This was achieved using a belt-driven system with a pulley,
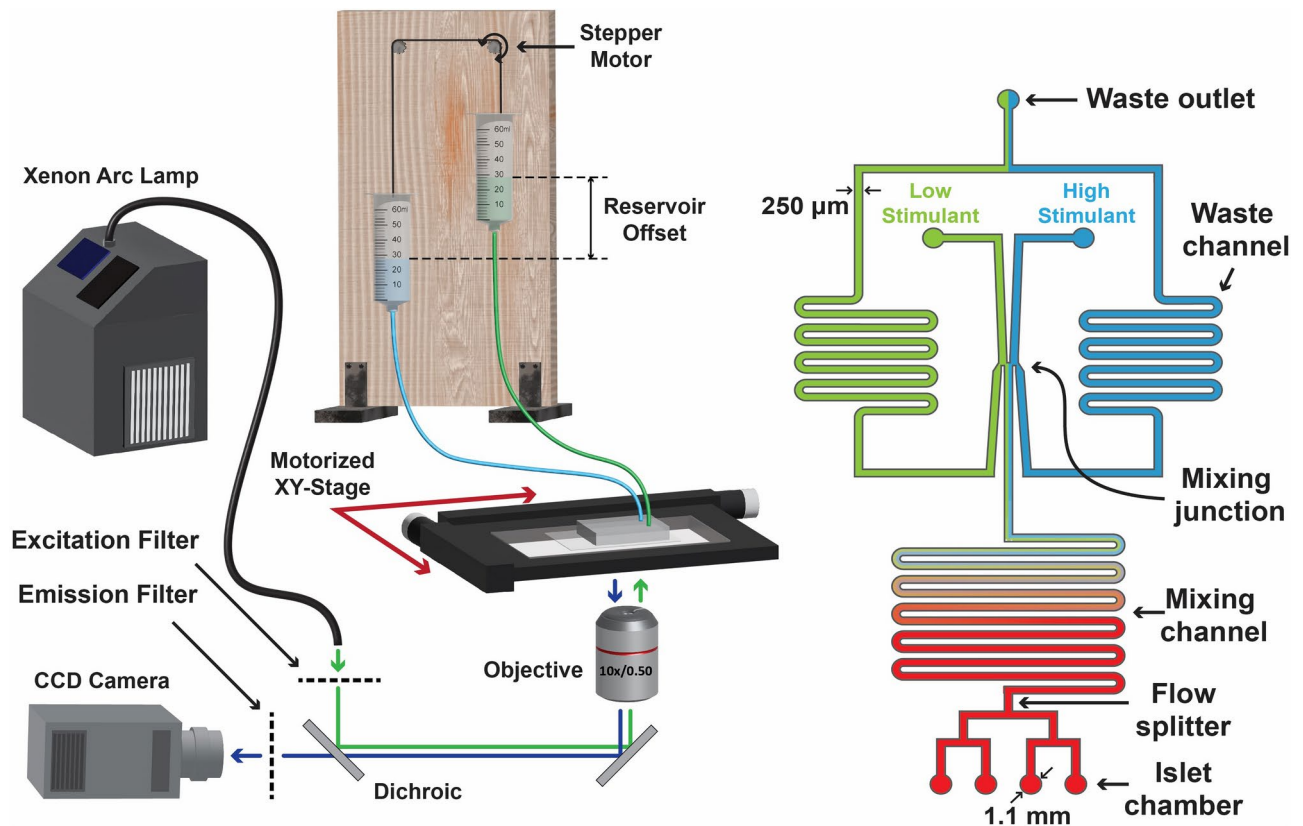

Fig. 1. Diagram of the experimental system. Starting from the left, light from a xenon arc lamp was made incident on an excitation filter to select the desired excitation wavelength. Excitation light was directed through a 10x objective via a dichroic mirror where it was focused onto the microfluidic device. Emission was collected through the same objective and directed through the dichroic mirror and an emission filter to a CCD camera. Gravity driven flow from two buffer reservoirs was used to drive fluid in the microfluidic device. The relative heights, and therefore flow rates, of the two reservoirs were controlled by a stepper motor, which dictated the concentration of stimulant or inhibitor delivered to the islets. The device design, shown on the right, had two inputs from the reservoirs leading to a mixing junction. The mixing channel was 200 mm long to provide sufficient time for homogenization of the inlet flows. The resulting solution was split to four chambers each of which contained between 5–6 islets. A motorized XY-stage moved the device such that each chamber was imaged.

with each end of the belt attached to one of the reservoirs, so that as one reservoir was raised, the other was lowered by the same amount. To automate the system, a stepper motor was used to turn the pulley an appropriate amount to change the fraction of stimulant delivered to the mixing channel, and ultimately, the concentration of reagent delivered to the islet chambers. This system allowed the flow rates from each inlet to be adjusted but the total flow rate into the microfluidic device was constant with minimal pressure pulses even when changing the ratio of input buffer flow rates. We have used this system to achieve high control over the buffer concentration delivered to individual islets[30,32]. Photographs of the microfluidic setup are shown in Fig. S1.

To increase throughput compared to our previous devices that used single islet chambers[30,32], the size of the islet chamber could have been increased, or multiple chambers used. However, as the chamber size increases, the time taken for buffer to wash out the chamber increases. By retaining smaller chambers, this washout time is minimized. A single large chamber with a large washout time would make it difficult to have all islets experience the same stimulant concentration at the same time[35]. To use a higher number of islet chambers than what we have used in the past, the input buffer flow rates were increased and a flow splitter was implemented at the end of the mixing channel to split the flow equally and deliver the fully mixed solution to 4 islet chambers where the liquid in the islet chambers is continuously replaced by the incoming flow[35]. The rationale for moving to 4 chambers was a trade off between throughput and simplicity in device design. Splitting a single microfluidic channel into two is relatively straightforward because the splitting junction is simple. The new design used two splits to deliver buffer to 4 islet chambers. The photomask used for fabrication of the microfluidic device is shown in Fig. S2. Higher numbers of chambers requires higher flow rates in the main channel which would lead to a longer mixing channel or to more complicated mixing structures. Also, the time required to load a larger number of chambers may become limiting. Currently, we required ≈ 2 min to load islets into each chamber, so a large number of chambers would not be feasible without a more rapid loading method.

To image all four chambers, the microfluidic device was mounted to a motorized XY-stage. Prior to initiating an experiment, the stage was manually positioned so that chamber 1 was in the field of view of the statically mounted objective. The position of the stage and the user defined ROIs of the islets were recorded. The stage was then moved to the next chamber, and the process repeated for the remaining chambers. Once imaging began, the program positioned the stage to the saved location for chamber 1, opened the shutter in the light source for the user defined exposure time, and took an image. If multiple images were required, as in Fura-2 imaging, the next image was then collected via the same process. The stage was then moved to the second chamber and the process repeated for all four chambers. This procedure enabled all chambers to be imaged within 10 s. During experiments, chambers were imaged every 20 s to reduce photobleaching.

Device characterization

As mentioned above, to accommodate a larger number of imaging chambers, the flow rate needed to be increased 4-fold compared to what we have used previously[30,32]. To achieve this higher flow, the reservoirs were raised higher above the microfluidic device than with previous devices and the mixing channel was made four times longer to maintain the required time for mixing. Because previous single-islet devices used a flow rate of 1 μL min^{-1} to be similar to what other in vitro systems have used[18,23,36], and to mimic in vivo flow rates[37], we aimed for a total flow rate of 4 μL min^{-1} in the mixing channel. To verify the flow rate after raising the reservoirs, the time taken to flow through the mixing channel was measured. As seen in Fig. 2a, a pulse of fluorescein, measured at the beginning and end of the mixing channel (red and blue curves, respectively), required 34 s to travel the channel. The volume of the mixing channel was calculated from the channel dimensions to be 2.5 μL, indicating a volumetric flow rate of 4.4 μL min^{-1}, close to the 4 μL min^{-1} that was desired. With this flow rate, the Reynolds number, Re, was calculated to be 2.2 confirming laminar flow.

With a higher flow rate used than in our previous devices, there was a possibility that the two input solutions may not have mixed prior to reaching the flow splitter. If this were to occur, then each islet chamber would receive a different concentration of stimulant. To test for complete mixing, a balanced salt solution (BSS) and BSS containing 500 nM fluorescein were delivered to the device via the two reservoirs. An image was taken at the end of the mixing channel and the fluorescence intensity across the width of the microfluidic channel was compared to an offline mixed preparation of 250 nM fluorescein. As seen in Fig. 2b, the normalized fluorescence intensities across the channel showed no difference between the solutions mixed offline (green line) and online (blue line) indicating that mixing was complete by the end of the mixing channel.

Fluid flow to the individual islet chambers is dependent on the resistance of each channel after the flow splitter. Since the channels leading to the islet chambers were short compared to those in the rest of the device, small deviations in the channels may produce different flow rates. To verify that buffer delivery to each chamber was identical, a pulse of fluorescein was delivered through the device and the fluorescence intensity in one of the chambers was measured every 0.5 s. This was repeated for all four chambers, and the delay time, t_d, defined as the time taken for the signal to rise 10% above baseline, was calculated for each (Fig. 2c). Along with t_d, the time required for a change in fluorescence to be affected, known as the response time t_r, was quantified as the time taken for the fluorescence intensity to change from 10% to 90% of the final value. The average ($\pm$ 1 standard deviation (SD)) t_d and t_r were found to be 46 ($\pm$ 0.4) s and 11.9 ($\pm$ 0.5) s, respectively. Both t_d and t_r for each chamber are summarized in Table 1. The normalized fluorescence intensities for each chamber were aligned and plotted in Fig. 2c. As seen, there was a high level of concurrence among chambers with RSDs between chambers of 0.77% and 3.4% for t_d and t_r, respectively. Such high concordance in the t_d and t_r among chambers is ideal because there will be negligible time differences between when stimulant is felt by islets in the different chambers, allowing a direct comparison of islet dynamics in different chambers.
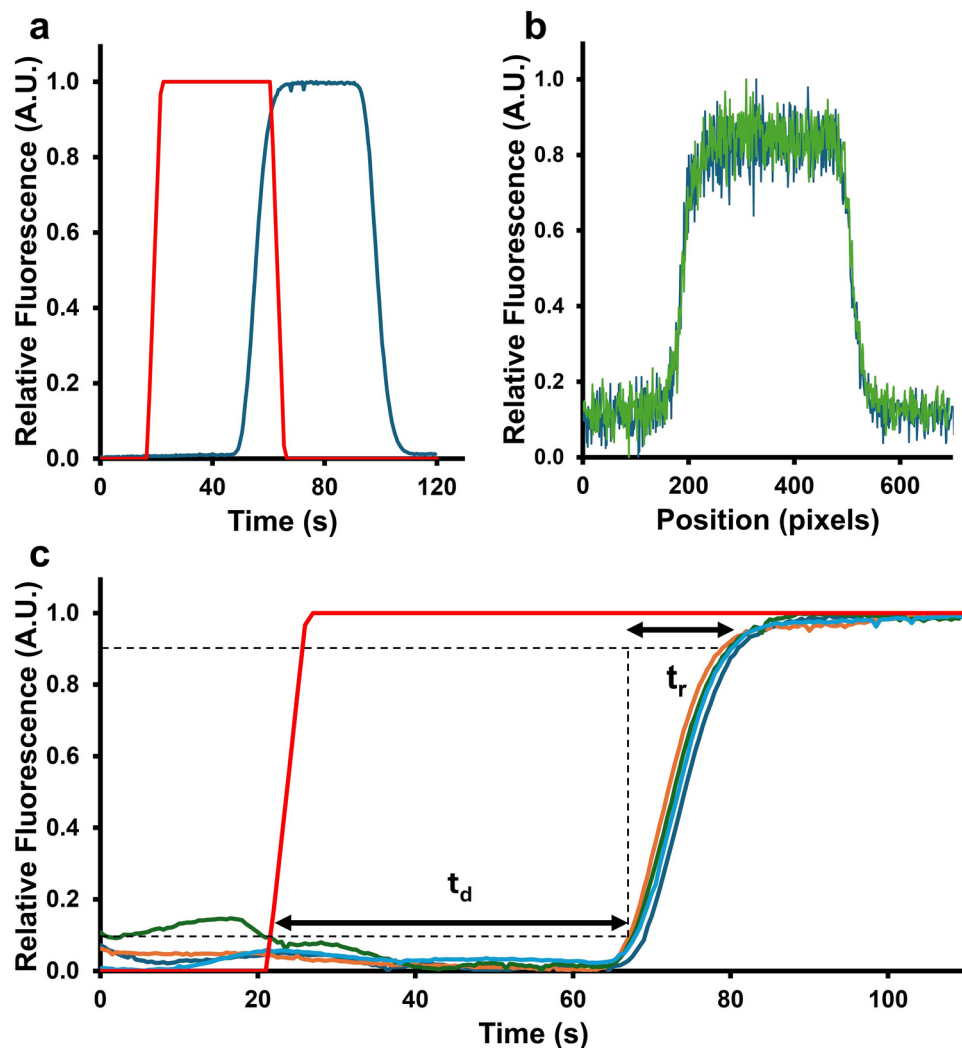
Fig. 2. Device characterization. (**a**) The red curve shows a fluorescein pulse delivered to the device and the blue curve shows the measured fluorescence at the end of the mixing channel. (**b**) Plots of relative fluorescence across the width of the channel immediately before the splitter are shown. Online and offline mixed 250 nM fluorescein is shown in blue and green, respectively. (**c**) A pulse of fluorescein delivered to the mixing junction is shown in red. The resulting fluorescence profiles in chambers 1–4 is shown by the dark blue, orange, green, and light blue curves, respectively. The 10% and 90% of fluorescence are highlighted as dashed lines. The delay time, t_d, and response time, t_r, are indicated.

Chamber No.	$t_d(s)$	$t_r(s)$
1	46.5	11.5
2	45.5	11.5
3	46.0	12.0
4	46.0	12.5

Table 1. t_d and t_r for individual imaging chamber.

Buffer delivery calibration

To calibrate the ratio of buffers needed for generating a range of stimulant concentrations, BSS containing fluorescein was perfused through one inlet and BSS without fluorescein was perfused through the other. The ratio of fluorescein-containing buffer entering the mixing channel was incrementally changed by increasing the height of its reservoir relative to the height of the other (i.e., the reservoir height offset). At each position tested, the fluorescence intensity was measured in each chamber. The fluorescence measured was normalized between 0 and 1 to obtain a relative fluorescence value. The step-wise increase in relative fluorescence caused by increasing

the reservoir offset over the course of 600 s is shown in Fig. 3a. All chambers followed the same curve, indicating a consistent response in all chambers.

During experiments with islets, a given stimulant concentration will be generated by changing the reservoir height offset a particular amount. The data from Fig. 3a were used to generate a plot of relative fluorescence as a function of reservoir offset (Fig. 3b). For each offset, the average relative fluorescence and the SD from the 4 chambers was calculated. At the extreme high and low values of relative fluorescence, there was a deviation from linearity due to the microfluidic design used. For example, at the 0.0 relative fluorescence point, flow from the reservoir containing only BSS pushes the flow from the reservoir containing fluorescein to the common waste outlet as described earlier. If the syringes are moved past that point so that an even higher flow rate from the BSS-only reservoir is generated, there will be no change in the measured fluorescence intensity. A similar saturation effect occurs on the high end of the scale, hence these points were not included in the calibration curve. A line of best fit was generated and produced an equation $Y = -1.5395 \times 10^{-4} X + 0.4931$, where X is the reservoir offset and Y is the relative fluorescence. The relative fluorescence can be equated to the % mixing, so the equation from the calibration curve can be used to calculate the required reservoir offset, X, to achieve a desired % mixing: $X = -6493Y + 3201$ where Y is the desired % mixing.

There is an additional benefit of measuring the fluorescence in the separate chambers. If the normalized fluorescence in the individual chambers did not overlap as in Fig. 3a, it would indicate incomplete mixing of the two input solutions in the mixing channel. The result shown here confirms complete mixing and could be used in lieu of the experiment described in Fig. 2a,b to reduce setup time. If mixing was not complete, the flow rate could have been decreased by reducing the height of both reservoirs in relation to the microfluidic device. The calibration would have to be performed again and the process repeated until there were sufficiently small differences between chambers. The criteria for accurate calibration was arbitrarily set as < 0.02 difference in relative fluorescence between all chambers for every calibration step. As a result, the difference in concentrations between chambers was < 1%.

Varying extracellular glucose conditions

Islets increase insulin secretion in response to elevated glucose and reduce insulin secretion when glucose levels are lower. β cells within islets secrete insulin in a pulsatile manner, and this pulsatility has important physiological consequences[38]. Pulsatile insulin secretion is due to electrical bursting activity that gives rise to oscillations in the intracellular Ca^{2+} concentration, $[Ca^{2+}]_i$[32,39]. Insulin is secreted in a Ca^{2+}-dependent manner, therefore $[Ca^{2+}]_i$ is often used as a surrogate for insulin secretion due to the ease at which it can be measured using fluorescent dyes[40–42].

To demonstrate the ability of the microfluidic system to map heterogeneity in islets, a titration of glucose was delivered to a group of islets and the $[Ca^{2+}]_i$ measured. To perform this assay, a 3 mM glucose solution in BSS and a 13 mM glucose solution in BSS were perfused through the two inlets of the microfluidic device and delivered to 21 Fura-2 loaded islets in the four imaging chambers (Fig. 4a–d). Initially, islets were perfused for 15 min with 3 mM glucose. Islets were inactive, showing no oscillatory activity and $[Ca^{2+}]_i$ below 50 nM (Fig. 4e).
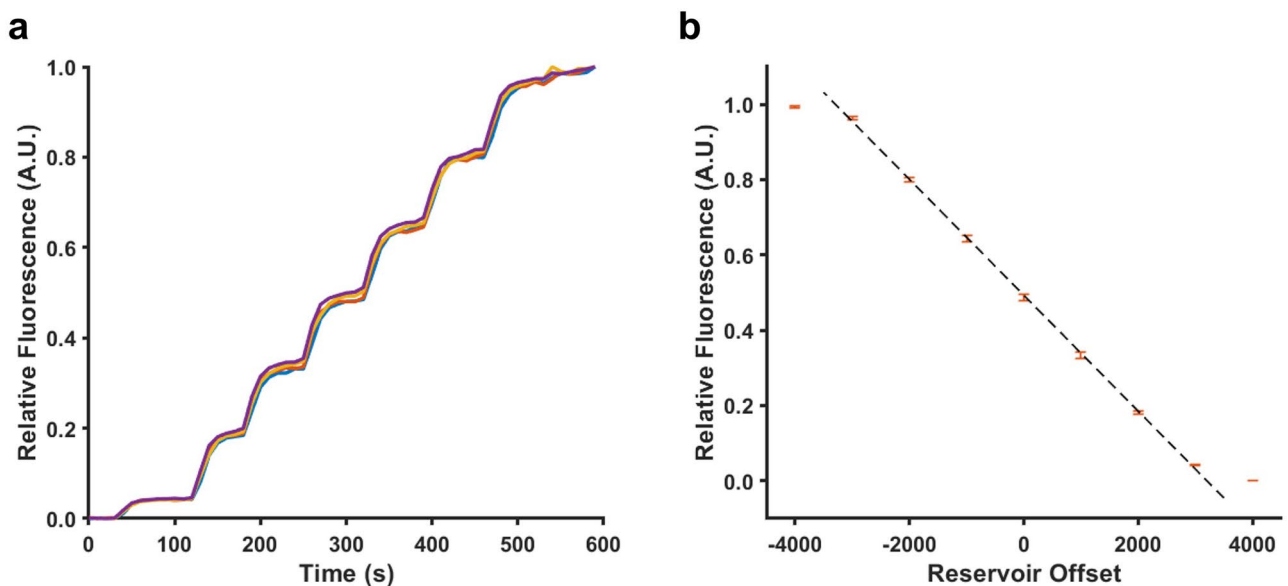

Fig. 3. Flow calibration. (**a**) A step-wise increase in fluorescein was delivered to all chambers and the relative fluorescence is plotted for chambers 1–4 in blue, red, yellow, and violet, respectively. Measurements were made every 2 s in sequential chambers. (**b**) A calibration curve of relative fluorescence against relative offset of the buffer reservoirs is shown. Orange points are the average of the fluorescence from the four chambers at each reservoir offset with error bars indicating ± 1 SD. The dashed line is a linear best fit, excluding the first and last points which deviated from linearity.
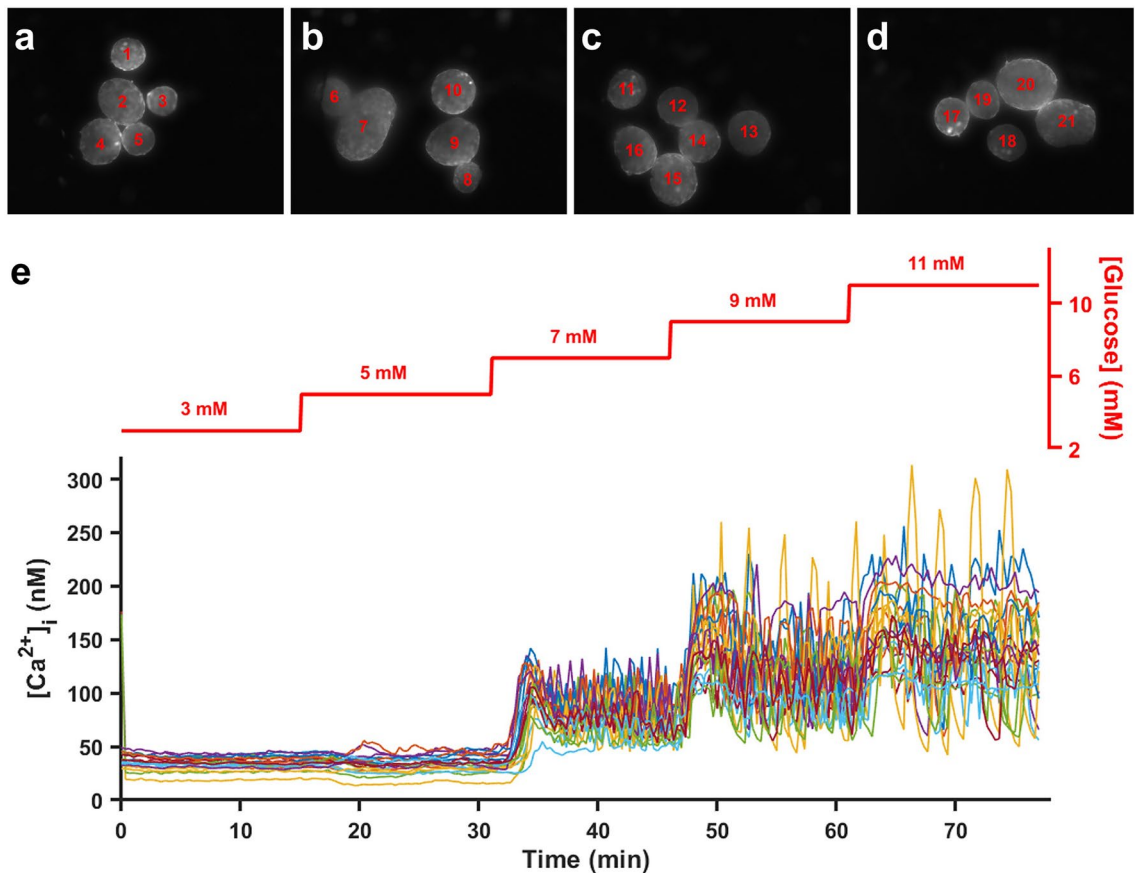
Fig. 4. Islet responses to step changes in glucose. (**a**–**d**) Images of islets loaded into chambers 1–4, respectively, are shown with 380 nm excitation. Islets are labeled 1–21 in red. (**e**) Dynamic $[Ca^{2+}]_i$ traces of all 21 islets over time under changing extracellular glucose conditions. The red bar at the top indicates the glucose concentration delivered over the course of the experiment.

The timing of the Fura-2 exposure inadvertently was 220 ms for the initial image instead of 150 ms. This artifact resulted in an artificially high $[Ca^{2+}]_i$ at the initial time point for these islets which can be seen in Fig. 4e. Nevertheless, the timing was consistent after that point. Glucose was then increased in 2 mM intervals every 15 min up to 11 mM. When glucose was increased to 5 mM, there was a small drop in $[Ca^{2+}]_i$ in some islets, corresponding to increased Ca^{2+} consumption by ATP-dependent processes. Past 7 mM glucose, islets became active with $[Ca^{2+}]_i$ oscillating. As glucose was further increased, the amplitude and baseline of these oscillations also increased. Some islets reached a tonic spiking state at 11 mM glucose where $[Ca^{2+}]_i$ never returned to a baseline level. No islets were observed to move during the course of the experiments which was likely due to their slight adhesion to the glass slide and to the gentle perfusion method not inducing pressure spikes even while concentrations were changed.

For assessing assay quality, a Z' factor was calculated according to the procedure outlined elsewhere[43]. Z' was calculated as:

$$Z' = 1 - \frac{3\sigma_c + 3\sigma_s}{|\overline{X}_s - \overline{X}_c|} \tag{1}$$

where σ_c and σ_s are the SD of the control and sample signals, respectively, and $\overline{X}_c$ and $\overline{X}_s$ are the average signal of the control and samples in the assay, respectively. A Z'-factor above 0.5 is considered an excellent assay[43]. The quantity used for evaluating the assay was the Ca^{2+} concentration averaged over a 10 min period, Ca_{avg}. The control, $\overline{X}_c$, was Ca_{avg} under the 3 mM glucose condition where there was no excitation of islets. The sample signal, $\overline{X}_s$, was the 13 mM glucose condition. The SD of the Ca_{avg} over the same periods were calculated and used as σ_c and σ_s. The Z'-factor was found to be 0.72 indicating high quality for this assay.

Traditional EC/IC$_{50}$ values for an inhibitory drug are calculated as the ensemble response from a population of cells. For islets, the same method is used[4,5,44,45]. For example, a group of islets are incubated under different conditions and their insulin secretions collected and quantified. The islets are then lysed and their intracellular insulin is quantified. The ratio of secreted to intracellular insulin gives a normalized secretion which is used to quantify the percent inhibition for a given drug or stimulant concentration[4,5,44,45]. In a population measurement,

the responses of individuals are averaged out, disallowing investigation of heterogeneity. With the newly developed device, a different approach can be used that allows for the determination of the response from individual islets, as well as the population, making it ideal for investigating islet heterogeneity.

The EC_{50} values of islets in response to glucose were calculated by fitting a logistic curve to the measured responses by least squared regression (Fig. 5). To obtain the response, the average $[Ca^{2+}]_i$ for the ensemble and each islet were normalized between zero and one. The black line is the ensemble fitted response curve while the black circles are the measured responses at the different glucose concentrations. The EC_{50} was found to be 7.4 mM for the ensemble. This corresponds well with literature EC_{50} values[46–48]. The EC_{50} curves for each individual islet were also calculated and plotted in red (Fig. 5). All EC_{50} values were within ± 0.6 mM of the ensemble value indicating tight control over the islets' glucose responses.

Heterogeneity of islet responses to a diazoxide challenge

Diazoxide (Dz) is a small molecule that opens ATP-sensitive K^+ channels (K_{ATP} channels), hyperpolarizing the β cell membrane and reducing $[Ca^{2+}]_i$ and thus insulin secretion[49]. The effect of Dz has been well documented on multiple mammalian species of islets including rat[5], mouse[50] and human[44]. To investigate the heterogeneity of islet responses to Dz, a titration of Dz was delivered to a group of 24 islets and the $[Ca^{2+}]_i$ measured. Fig. S3 shows the image of the islets used in the Dz assay. To perform this assay, a 200 µM solution of Dz in BSS with 20 mM glucose and a BSS solution with 20 mM glucose and no Dz were perfused through the two inlets of the microfluidic device. Initially, the Dz concentration was increased from 0 to 25 to 50 µM over a 45 min period (Fig. 6a). From this initial experiment, it was evident that $[Ca^{2+}]_i$ oscillations occurred at 0 µM Dz, as expected, but were partially inhibited during delivery of 25 µM Dz. The amplitude and frequency of oscillations were reduced during delivery of this concentration and oscillations were completely abolished by 50 µM. The concentration of Dz was returned to 0 µM to allow islets to begin oscillating again and a more focused titration of Dz was then applied. The Dz concentration was increased at 10 µM intervals and ended at 30 µM when no more oscillations were observed. In this second titration, the changes in the oscillations caused by the Dz were more gradual with reductions in amplitude visible at 10 µM. By 20 µM, oscillations were strongly inhibited, however there was still activity. All oscillations were abolished by 30 µM. A Z' score of 0.55 was calculated for the ensemble using Eq. 1, indicating an excellent assay. The control, $\overline{X}_c$, was Ca_{avg} under the 0 µM Dz condition where there was no inhibition of islets. The sample signal, $\overline{X}_s$, was the 30 µM Dz condition. σ_c and σ_s were the SD of Ca_{avg} over the same periods. Control experiments where the Dz vehicle (DMSO) was delivered in the same manner as Dz is shown in Fig. S4. The maximum DMSO concentration delivered to the islets was 0.04% and did not affect the $[Ca^{2+}]_i$ time courses.

The ensemble IC_{50} value was extracted by fitting the previously described logistic curve to the Ca_{avg} under each condition (Fig. 6b). The ensemble IC_{50} was found to be 10.2 µM. IC_{50} values have been calculated for Dz and Dz analogues using insulin secretion from groups of islets from different species[5,44]. These studies found a strong glucose dependence on the inhibitory effect of Dz, and our value is within the range of those found in these other studies. The heterogeneity of the individual islets is clearly demonstrated by plotting the individual islet IC_{50} curves along with that of the ensemble. There is a distribution of responses with varying sharpness of the curves and different half-response concentrations. In Fig. 6c, the individual IC_{50} values for each islet are plotted as black circles while the dashed lines in blue and red show the ensemble IC_{50} (10.3 µM) and average of the individual islet IC_{50} (10.9 µM), respectively.
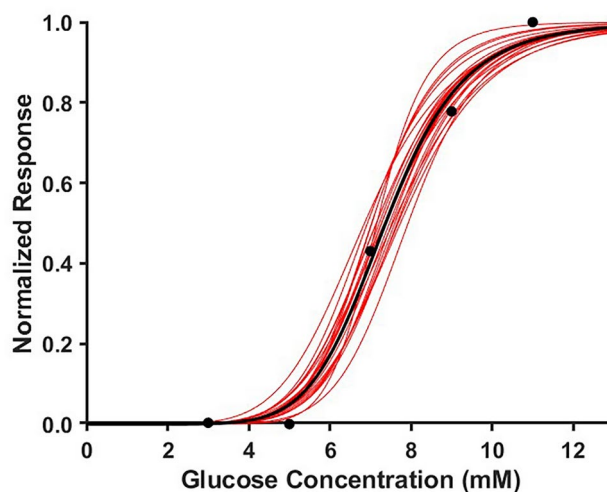

Fig. 5. Islet response to glucose. The ensemble response curve for glucose to the 21-islet population (black line) was fitted to the ensemble data (black points). The individual islet response curves are shown in red, fit to individual islet data.
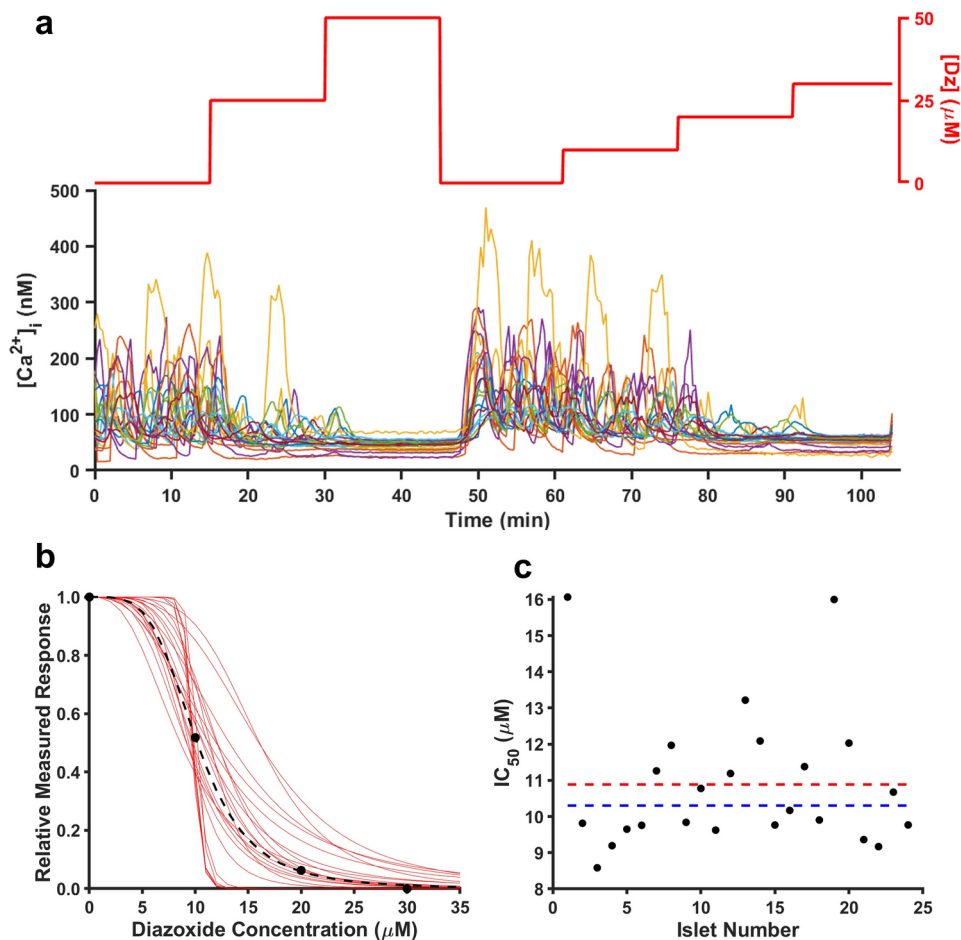
Fig. 6. Heterogeneous effects of Dz on islet activity. (**a**) The individual Ca^{2+} traces are shown with the Dz concentration shown in red at the top. The glucose concentration was held at 20 mM during the experiment. (**b**) A logistic curve described in Eq. 2 was fit (black dashed line) to the ensemble Ca_{avg} data points (black circles). Logistic fits were also used for individual islets (red curves). (**c**) IC_{50} values for each islet are plotted as black circles. The blue dashed line is the IC_{50} value for the ensemble and the red dashed line is the IC_{50} average of the individual islets.

Discussion

We have developed an automated microfluidic device enabling analysis of heterogeneity among an islet population with high accuracy and precision using a gravity-driven buffer perfusion system. Consistent delivery of a stimulant concentration of glucose across 4 chambers was accomplished and verified. High precision in the time required for stimulant to reach the chambers was achieved (0.77%), the response time (3.4%), and the difference in concentration of stimulant delivered to all four chambers (<1%).

The device was used to measure the response of a 21-islet population to increasing glucose levels and showed an ensemble EC_{50} value of 7.4 mM, similar to values found elsewhere[46–48]. The EC_{50} values of the individual islets were closely aligned to the ensemble average, with a maximum 0.6 mM deviation. The device was also used to measure IC_{50} values of Dz on a 24-islet population. The ensemble IC_{50} value of Dz was similar to other reports demonstrating concurrence with more established methods[5,44]. This system was also used to investigate the heterogeneous effects of the inhibitory drug on individual islets among the population. Most islets had responses similar to the population average, however 37% of islets deviated by 10% or greater from the average. As can be seen in Fig. 6c, there were outliers both below, and more prominently, above the ensemble values with 9 islets being more than 10% different from the average. The ensemble value is not the same as the average of the individual IC_{50}. If the IC_{50} values were randomly distributed around a mean, the average of the individual IC_{50} would be the same as the ensemble average. Because the average of the individual and ensemble were different indicates that the shape and asymmetry of the distribution plays a role in the ensemble response. There were a small number of islets that had a high tolerance to Dz compared to others which skewed the distribution.

Cellular heterogeneity is a growing focus of investigation with implications for disease progression, therapeutics, and cellular research. However, such studies require setups capable of resolving individual responses among a population, a challenge which often leads to increased experimental complexity. This platform is simple enough to be developed in other laboratories and capable of analyzing drug responses of cells, providing a tool

for the study of cellular heterogeneity. Islet heterogeneity has been identified as a factor in the development of diabetes and continues to be the subject of research aiming to elucidate the complex functionality of the endocrine system.

Methods

Chemicals and reagents

Sodium chloride (NaCl), calcium chloride ($CaCl_2$), magnesium chloride ($MgCl_2$), dimethyl sulfoxide (DMSO), and Fura 2 acetoxymethyl ester (AM) were acquired from Sigma-Aldrich (St. Louis, MO). Potassium chloride (KCl) and tricine were from VWR International (Radnor, PA). Sodium hydroxide (NaOH), glucose (dextrose), Dz, and bovine serum albumin (BSA) were purchased from Fisher Scientific (Pittsburgh, PA). Fetal bovine serum (FBS), penicillin-streptomycin, gentamicin, and Pluronic F-127 were from Thermo Fisher Scientific (Waltham, MA). Collagenase P was from Roche Diagnostics (Indianapolis, IN). RPMI 1640 was from Corning (Corning, NY). Polydimethylsiloxane (PDMS) and curing agent were from Dow Corning (Midland, MI). SU-8 photoresist was from Kayaku Advanced Materials (Westborough, MA). All solutions were made with ultrapure deionized (DI) water (Millipore, Bedford, MA). Glucose solutions were prepared in a balanced salt solution (BSS) composed of 125 mM NaCl, 5.9 mM KCl, 2.4 mM $CaCl_2$, 1.2 mM $MgCl_2$, and 25 mM tricine, at pH 7.4, with an additional 1 mg mL^{-1} BSA. Dz was initially dissolved in DMSO, then further diluted in BSS to the desired concentration for experiments.

Isolation and culture of islets

The islet isolation protocol was approved by the Florida State University Animal Care and Use Committee (Protocol No. 202000078). All methods are reported in accordance with ARRIVE guidelines[51]. Islets of Langerhans were obtained from 25-40 g male CD-1 mice (Charles River Laboratories, Wilmington, MA) by collagenase P digestion as described previously[52,53]. Isolated islets were incubated in RPMI 1640 medium with 11 mM glucose, L-glutamine, 10% FBS, 100 U mL^{-1} penicillin, 100 µg mL^{-1} streptomycin, and 10 µg mL^{-1} gentamicin at $37°C$ and 5% CO_2. Islets were used within 4 days after isolation. Islets from individual mice were not mixed during experiments.

Wafer and chip fabrication

The microfluidic device was a PDMS-glass hybrid with 2 inputs and 5 outlets. The PDMS layer was fabricated with soft photolitiography and SU-8 2050 photoresist. Briefly, $\sim$5 g of photoresist was poured onto a silicon wafer that had been cleaned in piranha solution composed of 50 mL H_2O_2 and 150 mL H_2SO_4. Please note, piranha solution is highly exothermic and care should be taken during its use. The wafer was spun for 10 s at 500 rpm with a ramp speed of 100 rpm s^{-1}, then for 30 s at 3200 rpm with a ramp speed of 300 rpm s^{-1}. The wafer was baked at $65°C$ for 1 min followed by 6 min at $95°C$ on two preheated hot plates. Edge beads were removed using an IPA soaked wipe by firmly rubbing the edge of the wafer. The photomask was aligned with the wafer then exposed with UV light from a flood exposure unit (OAI, Milpitas, CA) for 15 s at 11.8 mW cm^{-2}. The post-exposure bakes were 1 min at $65°C$ and 6 min at $95°C$. The channel outlines were visible in the SU-8 after the $65°C$ bake and the wafer was left to cool for 10 min at room temperature before developing. The wafer was developed for 5 min in SU-8 developer (Kayaku Advanced Materials, Westborough, MA) on an orbital shaker (Boekel Scientific, Feasterville ,PA). Undeveloped SU-8 was removed by rinsing with developer from a wash bottle, then with IPA to remove excess SU-8. The wafer was then baked again at $150°C$ for 10 min. The resulting channel dimensions on the master mold were 50 x 250 µm (height x width).

PDMS was mixed in a 10:1 ratio of base to curing agent and degassed before pouring over the mold in a 20 cm petri dish. Aluminum standoffs were placed into the PDMS at the location of the fluidic reservoirs. The PDMS was baked at $80°C$ for 80 min. The cured devices were cut out of the mold and inlets and outlets to the channels were fabricated using a 1.2 mm diameter hole punch. A glass cover slide (150 µm thick) was placed in a plasma oxidizer, along with the PDMS device, channel side up, and exposed to plasma for 70 s. Immediately after exposure, the device was firmly pressed to the glass, bonding the PDMS to the slide. The bonded device was further heated for 2 h at $80°C$, after which it was ready to use.

Optical system

An epiflourescent imaging system was used to measure both fluorescein and, as a measure of $[Ca^{2+}]_i$, Fura-2 fluorescence[42]. A xenon arc lamp with integrated filter wheel and shutter (Sutter Instruments, Novato, CA) was used for excitation of both fluorophores. The excitation light was guided via a liquid light guide to a collimator (CeramOptec, East Longmeadow, MA) and made incident on a dichroic mirror. Light then passed through a 10x, 0.5 numerical aperture (NA) objective lens (Nikon Instruments, Melville, NY) which focused light onto the microfluidic device. Emission was collected by the same objective, passed through the dichroic mirror, and through an emission filter. Images were then captured by a QIClick monochrome CCD camera (QImaging, Surrey, BC, Canada). For Fura-2 fluorescence, sequential excitation was performed using 340 ± 5 nm and 380 ± 5 nm excitation filters (Omega Optical 340AF15 and 380AF15, Brattleboro, VT), a 409 nm dichroic mirror (Semrock, Rochester, NY), and a 510 ± 84 nm emission filter (Semrock). For fluorescein imaging experiments, a 482 ± 35 nm excitation filter (Semrock) was used with a 506 nm dichroic (Semrock) and a 536 ± 40 nm emission filter (Semrock).

The microfluidic device was mounted on top of a motorized XY-stage (Zaber, Vancouver, BC) which was controlled by a custom LabVIEW program (National Instruments, Austin, TX). During experiments, four imaging locations were selected (one for each imaging chamber) and the stage traversed between locations with images collected at each.

To measure $[\text{Ca}^{2+}]_i$, 1 µL of 5 mM Fura 2 AM in DMSO and 1 µL of Pluronic F-127 in DMSO were added to 1.998 mL of RPMI 1640 medium. Islets were incubated in this solution for 40 min at 37 °C and 5% CO_2. After incubation, islets were rinsed in a petri dish that contained pre-warmed BSS with 10 mM glucose. Groups of 5-8 islets were removed from the petri dish using a 10 µL gel loading pipette tip. The tip was submerged just below the liquid in the imaging chamber and the islets were pipetted in. Flow was continuously delivered to the chambers during loading. Islets settled onto the glass slide at the bottom of the chambers after ~20 s. Regions of interest (ROIs) were selected for each islet, as well as a background ROI for each chamber, prior to initiating the experiment. The background subtracted fluorescence emission for each islet after 340 nm excitation was divided by the background subtracted emission after 380 nm excitation to generate the fura ratio. $[\text{Ca}^{2+}]_i$ was calculated from the fura ratio using a calibration curve, as has been described previously[54].

Gravity system

The gravity-based flow system was similar to that described elsewhere[33,34,53,55,56]. Briefly, perfusion through the microfluidic channels was gravity driven by suspending reservoirs of buffer above the device. This generated hydrostatic pressure at the inlets which drove fluid flow through the device. Two 60 mL syringes with plungers removed acted as the reservoirs and were used to hold 10 mL of low and high concentration stimulant solutions in BSS. The reservoirs were connected to the two inputs of the microfluidic system via Teflon tubing. The reservoirs were attached to a rubber belt which was suspended on a pulley system. The belt passed over a stepper motor (Phidgets, Calgary, AB, Canada). The stepper motor was controlled by a custom LabVIEW program which rotated the motor and moved the rubber belt on the pulley, and hence the height of the reservoirs, enabling differential flow rates from each reservoir while maintaining a constant total flow rate into the device. Photographs of the microfluidic setup are shown in Fig. S1.

EC/IC$_{50}$ determination

EC/IC$_{50}$ values for each islet were calculated by averaging the $[\text{Ca}^{2+}]_i$ for each stimulant or inhibitor concentration over a 10 min period. These average $[\text{Ca}^{2+}]_i$ values for each islet j, Ca_{avg_j}, were then normalized between 0 and 1. The EC/IC$_{50}$ was then determined by fitting a four-parameter logistic curve to the normalized response at each concentration using:

$$Y = \frac{\min - \max}{1 + (\frac{X}{EC/IC_{50}})^h} + \max \tag{2}$$

where Y is the normalized response, $\max$ and $\min$ are the maximum and minimum response, X is the concentration of stimulant or inhibitor, EC/IC$_{50}$ is the concentration at 50% maximal value and h is a parameter defining the steepness of the logistic curve (i.e., Hill coefficient). Since the % response is normalized between 1 and 0, $\max$ and $\min$ are always 1 and 0, respectively. EC/IC$_{50}$ and h, were optimized to minimize the square of the sum of the residuals between the curve generated from Eq. 2 and the experimental data. The fitting was performed for each islet using a Matlab script (MATLAB R2023b, Natick, MA). The same process was used for fitting the ensemble EC/IC$_{50}$ curve to the average of the individual $[\text{Ca}^{2+}]_i$ traces.

Data availability

Data generated during this study is available upon reasonable request from the corresponding author.

References

1. Center for Disease Control and Prevention, National Diabetes Statistics Report, May 15, 2024. https://www.cdc.gov/diabetes/php/data-research/index.html. Accessed: 2024-06-10.
2. Da Silva Xavier, G. The cells of the islets of Langerhans. *J. Clin. Med.* **7**, 54 (2018).
3. Blahova, J. et al. Pharmaceutical drugs and natural therapeutic products for the treatment of type 2 diabetes mellitus. *Pharmaceuticals* **14**, 806 (2021).
4. Jonas, J. C. et al. Multiple effects and stimulation of insulin secretion by the tyrosine kinase inhibitor genistein in normal mouse islets. *Br. J. Pharmacol.* **114**, 872–880 (1995).
5. Lebrun, P. et al. A potent diazoxide analogue activating ATP-sensitive K^+ channels and inhibiting insulin release. *Diabetologia* **43**, 723–732 (2000).
6. Johnson, J. D. et al. Increased islet apoptosis in Pdx1$^{+/-}$ mice. *J. Clin. Invest.* **111**, 1147–1160 (2003).
7. Kolic, J. et al. Differential effects of voclosporin and tacrolimus on insulin secretion from human islets. *Endocrinology* **161**, 1–14 (2020).
8. Dorrell, C. et al. Human islets contain four distinct subtypes of β cells. *Nat. Commun.* **7**, 11756 (2016).
9. Katsuta, H. et al. Subpopulations of GFP-marked mouse pancreatic β-cells differ in size, granularity, and insulin secretion. *Endocrinology* **153**, 5180–5187 (2012).
10. Dishinger, J. F., Reid, K. R. & Kennedy, R. T. Quantitative monitoring of insulin secretion from single islets of Langerhans in parallel on a microfluidic chip. *Anal. Chem.* **81**, 3119–3127 (2009).
11. Wang, Y., Adeoye, D. I., Wang, Y. J. & Roper, M. G. Increasing insulin measurement throughput by fluorescence anisotropy imaging immunoassays. *Analytica. Chim. Acta.* **1212**, 339942 (2022).
12. Roscioni, S. S., Migliorini, A., Gegg, M. & Lickert, H. Impact of islet architecture on β-cell heterogeneity, plasticity and function. *Nat. Rev. Endocrinol.* **12**, 695–709 (2016).
13. Bratusch-Marrain, P. R., Komjati, M. & Waldhäusl, W. K. Efficacy of pulsatile versus continuous insulin administration on hepatic glucose production and glucose utilization in type I diabetic humans. *Diabetes* **35**, 922–926 (1986).
14. Regeenes, R. & Rocheleau, J. V. Twenty years of islet-on-a-chip: Microfluidic tools for dissecting islet metabolism and function. *Lab Chip* **24**, 1327–1350 (2024).

15. Adablah, J. E., Vinson, R., Roper, M. G. & Bertram, R. Synchronization of pancreatic islets by periodic or non-periodic muscarinic agonist pulse trains. *PLoS ONE* **14**, e0211832 (2019).
16. Rocheleau, J. V., Walker, G. M., Head, W. S., McGuinness, O. P. & Piston, D. W. Microfluidic glucose stimulation reveals limited coordination of intracellular Ca^{2+} activity oscillations in pancreatic islets. *Proc. Natl. Acad. Sci.* **101**, 12899–12903 (2004).
17. Lee, C. J. et al. Relations between glucose and D-amino acids in the modulation of biochemical and functional properties of rodent islets of Langerhans. *ACS Omega* **8**, 47723–47734 (2023).
18. Easley, C. J., Rocheleau, J. V., Head, W. S. & Piston, D. W. Quantitative measurement of zinc secretion from pancreatic islets with high temporal resolution using droplet-based microfluidics. *Anal. Chem.* **81**, 9086–9095 (2009).
19. Schrell, A. M. et al. Online fluorescence anisotropy immunoassay for monitoring insulin secretion from islets of Langerhans. *Anal. Methods* **9**, 38–45 (2017).
20. Li, X., Hu, J. & Easley, C. J. Automated microfluidic droplet sampling with integrated, mix-and-read immunoassays to resolve endocrine tissue secretion dynamics. *Lab Chip* **18**, 2926–2935 (2018).
21. Shackman, J. G., Dahlgren, G. M., Peters, J. L. & Kennedy, R. T. Perfusion and chemical monitoring of living cells on a microfluidic chip. *Lab Chip* **5**, 56–63 (2005).
22. Wu Jin, P., Rousset, N., Hierlemann, A. & Misun, P. M. A microfluidic hanging-drop-based islet perifusion system for studying glucose-stimulated insulin secretion from multiple individual pancreatic islets. *Front. Bioeng. Biotechnol.* **9**, 674431 (2021).
23. Mohammed, J. S., Wang, Y., Harvat, T. A., Oberholzer, J. & Eddington, D. T. Microfluidic device for multimodal characterization of pancreatic islets. *Lab Chip* **9**, 97–106 (2009).
24. Xing, Y. et al. A pumpless microfluidic device driven by surface tension for pancreatic islet analysis. *Biomed. Microdevice* **18**, 80 (2016).
25. Nunemaker, C. S. et al. Glucose metabolism, islet architecture, and genetic homogeneity in imprinting of $[Ca^{2+}]_i$ and insulin rhythms in mouse islets. *PLoS ONE* **4**, e8428 (2009).
26. Schulze, T. et al. A 3D microfluidic perfusion system made from glass for multiparametric analysis of stimulus-secretioncoupling in pancreatic islets. *Biomed. Microdevices* **19**, 47 (2017).
27. Adewola, A. F. et al. Microfluidic perifusion and imaging device for multi-parametric islet function assessment. *Biomed. Microdevice* **12**, 409–417 (2010).
28. Wang, X., Yi, L. & Roper, M. G. Microfluidic device for the measurement of amino acid secretion dynamics from murine and human islets of Langerhans. *Anal. Chem.* **88**, 3369–3375 (2016).
29. Davis, J. J. et al. Simultaneous monitoring of multiple hormones from human islets of Langerhans using solid-phase extraction-mass spectrometry. *Anal. Bioanal. Chem.* **415**, 5671–5680 (2023).
30. Dhumpa, R., Truong, T. M., Wang, X., Bertram, R. & Roper, M. G. Negative feedback synchronizes islets of Langerhans. *Biophys. J.* **106**, 2275–2282 (2014).
31. Dhumpa, R., Truong, T. M., Wang, X. & Roper, M. G. Measurement of the entrainment window of islets of Langerhans by microfluidic delivery of a chirped glucose waveform. *Integr. Biol.* **7**, 1061–1067 (2015).
32. Bruce, N. et al. Coordination of pancreatic islet rhythmic activity by delayed negative feedback. *Am. J. Physiol.* **323**, 492–502 (2022).
33. Ferry, M., Razinkov, I. & Hasty, J. Chapter fourteen - microfluidics for synthetic biology: From design to execution. In Voigt, C. (ed.) *Synthetic Biology, Part A*, vol. 497 of *Methods in Enzymology*, 295–372 (Academic Press, 2011).
34. Prindle, A. et al. Rapid and tunable post-translational coupling of genetic circuits. *Nature* **508**, 387–391 (2014).
35. Zhang, X., Dhumpa, R. & Roper, M. G. Maintaining stimulant waveforms in large-volume microfluidic cell chambers. *Microfluid. Nanofluid.* **15**, 65–71 (2013).
36. Silva, P. N., Green, B. J., Altamentova, S. M. & Rocheleau, J. V. A microfluidic device designed to induce media flow throughout pancreatic islets while limiting shear-induced damage. *Lab Chip* **13**, 4374–4384 (2013).
37. Nyman, L. R. et al. Real-time, multidimensional in vivo imaging used to investigate blood flow in mouse pancreatic islets. *J. Clin. Invest.* **118**, 3790–3797 (2008).
38. Matthews, D. R., Naylor, B. A., Jones, R. G., Ward, G. M. & Turner, R. C. Pulsatile insulin has greater hypoglycemic effect than continuous delivery. *Diabetes* **32**, 617–621 (1983).
39. Marinelli, I., Vo, T., Gerardo-Giorda, L. & Bertram, R. Transitions between bursting modes in the integrated oscillator model for pancreatic β-cells. *J. Theor. Biol.* **454**, 310–319 (2018).
40. Jonas, J. C., Gilon, P. & Henquin, J. C. Temporal and quantitative correlations between insulin secretion and stably elevated or oscillatory cytoplasmic Ca^{2+} in mouse pancreatic β-cells. *Diabetes* **47**, 1266–1273 (1998).
41. Gilon, P. & Henquin, J. C. Distinct effects of glucose on the synchronous oscillations of insulin release and cytoplasmic ca^{2+} concentration measured simultaneously in single mouse islets. *Endocrinology* **136**, 5725–5730 (1995).
42. Yi, L., Bandak, B., Wang, X., Bertram, R. & Roper, M. G. Dual detection system for simultaneous measurement of intracellular fluorescent markers and cellular secretion. *Anal. Chem.* **88**, 10368–10373 (2016).
43. Zhang, J. H., Chung, T. D. Y. & Oldenburg, K. R. A simple statistical parameter for use in evaluation and validation of high throughput screening assays. *J. Biomol. Screen.* **4**, 67–73 (1999).
44. Henquin, J. C., Dufrane, D., Gmyr, V., Kerr-Conte, J. & Nenquin, M. Pharmacological approach to understanding the control of insulin secretion in human islets. *Diabetes Obes. Metab.* **19**, 1061–1070 (2017).
45. Amin, J. et al. A simple, reliable method for high-throughput screening for diabetes drugs using 3D β-cell spheroids. *J. Pharmacol. Toxicol. Methods* **82**, 83–89 (2016).
46. Antunes, C. M., Salgado, A. P., Rosário, L. M. & Santos, R. M. Differential patterns of glucose-induced electrical activity and intracellular calcium responses in single mouse and rat pancreatic islets. *Diabetes* **49**, 2028–2038 (2000).
47. Rebelato, E., Santos, L. R., Carpinelli, A. R., Rorsman, P. & Abdulkader, F. Short-term high glucose culture potentiates pancreatic beta cell function. *Sci. Rep.* **8**, 13061 (2018).
48. Low, J. T. et al. Glucose principally regulates insulin secretion in mouse islets by controlling the numbers of granule fusion events per cell. *Diabetologia* **56**, 2629–2637 (2013).
49. Dukes, I. D. & Philipson, L. H. K^+ channels: Generating excitement in pancreatic β-cells. *Diabetes* **45**, 845–853 (1996).
50. Gembal, M., Gilon, P. & Henquin, J. C. Evidence that glucose can control insulin release independently from its action on ATP-sensitive K^+ channels in mouse β cells. *J. Clin. Invest.* **89**, 1288–1295 (1992).
51. Percie du Sert, N. et al. The arrive guidelines 2.0: Updated guidelines for reporting animal research. *PLoS Biol.* **18**, 1–12 (2020).
52. Roper, M. G., Shackman, J. G., Dahlgren, G. M. & Kennedy, R. T. Microfluidic chip for continuous monitoring of hormone secretion from live cells using an electrophoresis-based immunoassay. *Anal. Chem.* **75**, 4711–4717 (2003).
53. Yi, L. et al. Integrated perfusion and separation systems for entrainment of insulin secretion from islets of Langerhans. *Lab Chip* **15**, 823–832 (2015).
54. Grynkiewicz, G., Poenie, M. & Tsien, R. Y. A new generation of Ca^{2+} indicators with greatly improved fluorescence properties. *J. Biol. Chem.* **260**, 3440–3450 (1985).
55. Lomasney, A. R., Yi, L. & Roper, M. G. Simultaneous measurements of insulin release dynamics from single islets of langerhans in response to 5-palmitic acid hydroxy stearic acid. *Anal. Chem.* **85**, 7919–7925 (2013).
56. Bandak, B., Yi, L. & Roper, M. G. Microfluidic-enabled quantitative measurements of insulin release dynamics from single islets of langerhans in response to 5-palmitic acid hydroxy stearic acid. *Lab Chip* **18**, 2873–2882 (2018).

Acknowledgements

Author contributions

J.T.: designed research, performed research, analyzed data, and wrote manuscript. R.B. designed research, analyzed data, and edited the manuscript. M.G.R. designed research, analyzed data, and edited the manuscript.

Competing interests

The authors declare no competing interests.

Additional information

Supplementary Information The online version contains supplementary material available at https://doi.org/10.1038/s41598-024-75340-1.

Correspondence and requests for materials should be addressed to M.G.R.

Reprints and permissions information is available at www.nature.com/reprints.

Publisher's note Springer Nature remains neutral with regard to jurisdictional claims in published maps and institutional affiliations.